ISSN 1674-1056
http://cpb.iphy.ac.cn
http://iopscience.iop.org/cpb
中国物理 B
Chinese Physics
中国物理 Chinese Physics B

Prediction of high-mobility two-dimensional electron gas at $KTaO_3$-based heterointerfaces

Fu-Ning Wang(王芙凝), Ji-Chao Li(李吉超), Yi Li(李宜), Xin-Miao Zhang(张鑫淼), Xue-Jin Wang(王学晋), Yu-Fei Chen(陈宇飞), Jian Liu(刘剑), Chun-Lei Wang(王春雷), Ming-Lei Zhao(赵明磊), Liang-Mo Mei(梅良模)

Citation: Chin. Phys. B . 2019, 28(4): 047101. **doi:** 10.1088/1674-1056/28/4/047101
Journal homepage: http://cpb.iphy.ac.cn; http://iopscience.iop.org/cpb

What follows is a list of articles you may be interested in

Theoretical design of multifunctional half-Heusler materials based on first-principles calculations

Xiuwen Zhang(张秀文)
Chin. Phys. B . 2018, 27(12): 127101. **doi:** 10.1088/1674-1056/27/12/127101

Effect of Mn doping on mechanical properties and electronic structure of WCoB ternary boride by first-principles calculations

Tong Zhang(张桐), Hai-Qing Yin(尹海清), Cong Zhang(张聪), Xuan-Hui Qu(曲选辉), Qing-Jun Zheng(郑清军)
Chin. Phys. B . 2018, 27(10): 107101. **doi:** 10.1088/1674-1056/27/10/107101

The effects of combining alloying elements on the elastic properties of *γ*-Ni in Ni-based superalloy: High-throughput first-principles calculations

Baokun Lu(路宝坤), Chongyu Wang(王崇愚)
Chin. Phys. B . 2018, 27(7): 077104. **doi:** 10.1088/1674-1056/27/7/077104

Structural, electronic, elastic, and thermal properties of $CaNiH_3$ perovskite obtained from first-principles calculations

S Benlamari, H Bendjeddou, R Boulechfar, S Amara Korba, H Meradji, R Ahmed, S Ghemid, R Khenata, S Bin Omran
Chin. Phys. B . 2018, 27(3): 037104. **doi:** 10.1088/1674-1056/27/3/037104

Uniaxial strain-modulated electronic structures of Cd*X* (*X*=S, Se, Te) from first-principles calculations: A comparison between bulk and nanowires

Linlin Xiang(相琳琳), Shenyuan Yang(杨身园)
Chin. Phys. B . 2017, 26(8): 087103. **doi:** 10.1088/1674-1056/26/8/087103

Prediction of high-mobility two-dimensional electron gas at $KTaO_3$-based heterointerfaces*

Fu-Ning Wang(王芙凝), Ji-Chao Li(李吉超)†, Yi Li(李宜), Xin-Miao Zhang(张鑫淼), Xue-Jin Wang(王学晋), Yu-Fei Chen(陈宇飞), Jian Liu(刘剑), Chun-Lei Wang(王春雷), Ming-Lei Zhao(赵明磊), and Liang-Mo Mei(梅良模)

School of Physics, Shandong University, Jinan 250100, *China*

(Received 27 December 2018; revised manuscript received 13 February 2019; published online 5 March 2019)

First-principles calculations are performed to explore the possibility of generating the two-dimensional electron gas (2DEG) at the interface between $LaGaO_3/KTaO_3$ and $NdGaO_3/KTaO_3$ (001) heterostructures. Two different models — *i.e.*, the superlattice model and the thin film model — are used to conduct a comprehensive investigation of the origin of charge carriers. For the symmetric superlattice model, the $LaGaO_3$ (or $NdGaO_3$) film is nonpolar. The 2DEG with carrier density on the order of 10^{14} cm^{-2} originates from the Ta d_{xy} electrons contributed by both $LaGaO_3$ (or $NdGaO_3$) and $KTaO_3$. For the thin film model, large polar distortions occur in the $LaGaO_3$ and $NdGaO_3$ layer, which entirely screens the built-in electric field and prevents electrons from transferring to the interface. Electrons of $KTaO_3$ are accumulated at the interface, contributing to the formation of the 2DEG. All the heterostructures exhibit conducting properties regardless of the film thickness. Compared with the Ti d_{xy} electrons in $SrTiO_3$-based heterostructures, the Ta d_{xy} electrons have small effective mass and they are expected to move with higher mobility along the interface. These findings reveal the promising applications of 2DEG in novel nanoelectronic devices.

Keywords: 2DEG, first-principles calculation, interface

PACS: 71.10.Ca, 63.20.dk, 67.30.hp **DOI:** 10.1088/1674-1056/28/4/047101

1. Introduction

Oxide heterostructures have emerged as a powerful platform for discovering novel interfacial properties, such as magnetism[1] and superconductivity.[2,3] One major area of interest within the field is the two-dimensional electron gas (2DEG) discovered at the interface between two insulators: $LaAlO_3$ (LAO) and $SrTiO_3$ (STO).[4] The 2DEG with high sheet carrier density is particularly notable for its potential applications in nanoelectronic devices.[5] The mechanism of formation of the 2DEG remains a primary concern and several theories have been proposed. Electronic reconstruction due to the polar discontinuity,[6–8] oxygen vacancies in STO,[9–12] and the cation intermixing across the interface[13,14] have been considered to be responsible for the interfacial conductivity. The origin of the 2DEG formed at the interface has been investigated both in theory[15–18] and experiment.[9,19–24]

So far, most of the investigations of the 2DEG focus on the oxide heterostructures based on STO substrate, such as the following

LAO/STO, $LaTiO_3/SrTiO_3$ (LTO/STO),[25,26]

$LaGaO_3/SrTiO_3$ (LGO/STO),[27]

$GdTiO_3/SrTiO_3$ (GTO/STO),[28]

$NdAlO_3/SrTiO_3$ (NAO/STO),[29]

and $NdGaO_3/SrTiO_3$ (NGO/STO).[30–33]

Although lots of STO-based heterostructures host high-density 2DEG, low room-temperature mobility (less than 10 $cm^2/V{\cdot}s$)[4,9,26,28,34] largely constrains their development and practical application in a general case. Compared with STO, $KTaO_3$ (KTO) is also a widely used substrate material and its mobility at room temperature is 30 $cm^2/V{\cdot}s$.[35] One could speculate that the mobility of the 2DEG in heterostructures based on KTO could be further improved. Zou *et al.*[36] first observed the conducting interface in LTO/KTO. Surprisingly, the electron mobility in the LTO/KTO heterostructure is as high as 21 $cm^2/V{\cdot}s$ at room temperature, several times larger than that of doped STO. Later the high-quality 2DEG has been observed at the amorphous LAO/KTO heterointerface.[37] Recently, the epitaxial films of the EuO have also been successfully grown on KTO crystals by using the molecular beam epitaxy, and the 2DEG is observed with a high mobility of 11.8 $cm^2/V{\cdot}s$ at room temperature.[38] In addition to experiments, it has been theoretically predicted that the 2DEG can be created at the interface of LAO/KTO.[39] However, the 2DEG formed at the KTO-based heterointerfaces has been seldom studied in theory. Therefore, theoretical investigations on the new KTO-based heterostructures will help to discover superior 2DEG system with higher mobility.

In this article, a comprehensive study of LGO/KTO and NGO/KTO heterostructures in two different models is carried out by using first-principles calculations to explore the

*Project supported by the National Basic Research Program of China (Grant No. 2013CB632506) and the National Natural Science Foundation of China (Grant Nos. 11374186, 51231007, and 51202132).

†Corresponding author. E-mail: lijichao@sdu.edu.cn

© 2019 Chinese Physical Society and IOP Publishing Ltd

possibility of generating the 2DEG at the interfaces. First, it is found that the 2DEG can be produced at LGO/KTO and NGO/KTO heterointerface in the symmetric superlattice model. The electrical properties are studied and the origin of the 2DEG is discussed. Then, in the thin film model we find that the metallic properties of LGO/KTO and NGO/KTO heterointerface are independent of the film thickness. The reason why there is no transition from insulating to metallic for LGO/KTO nor NGO/KTO in the thin film model is explained and the stability of the interface is explored.

2. Models and computational details

For both LGO/KTO and NGO/KTO heterostructures, two different models, *i.e.*, the superlattice and the thin film model, are used to investigate the geometrical and electronic structures, as shown in Fig. 1. Since it has been experimentally proven that the KO surface can be hardly obtained for (001) oriented KTO,[40] we only focus on the $(AO)^{+}/(TaO_2)^{+}$ (A = La and Nd) interface. In the superlattice model, the $(AGO)_{5.5}/(KTO)_{5.5}$ superlattice containing 5.5 unit cells (u.c.) of AGO and 5.5 u.c. of KTO was studied. Owing to an additional AO or TaO_2 layer in AGO or KTO, there are two identical n-type interfaces. In the thin film model, an $(AGO)_m/(KTO)_{6.5}/(AGO)_m$ supercell consisting of 6.5 u.c. of KTO and m u.c. of symmetric AGO film along the (001) direction was employed. $1 \leq m \leq 10$ and m is an integer. To minimize the interaction between neighboring surfaces, periodic slabs were separated in the z direction by 15 Å of vacuum. The density functional theory calculations were performed by using the projector augmented wave method as implemented in the Vienna *ab initio* Simulation Package (VASP)[41] with projector-augmented wave (PAW) potential. The electronic exchange correlation potential was parameterized in the generalized gradient approximation (GGA).[42] In all calculations the plane wave energy cut-off was 400 eV and the reciprocal space was described by the Monkhorst–Pack scheme.[43] The in-plane lattice constants were fixed at the experimental lattice constant of bulk-KTO. The internal positions of the atoms were allowed to relax until the force acting on atoms was less than 0.01 eV/Å.

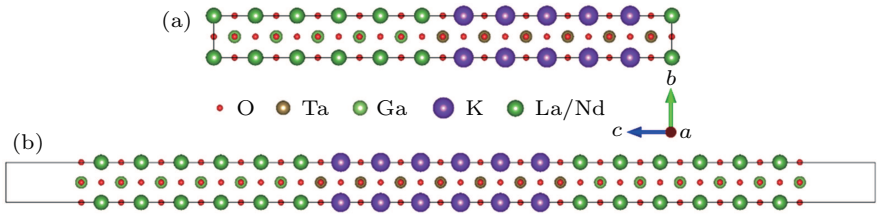


Fig. 1. Schematic illustration of different models in this study: (a) $(AGO)_{5.5}/(KTO)_{5.5}$ (A = La or Nd) superlattices model and (b) $(AGO)_6/(KTO)_{6.5}/(AGO)_6$ supercell.

3. Results and discussion

3.1. Bulk compounds

KTO has a cubic phase with space group $Pm\bar{3}m$, and its experimental lattice constant is 3.989 Å.[44] In contrast, LGO and NGO both exhibit an orthorhombic phase, and they can be regarded as pseudocubic structures with lattice constant of 3.874 Å[27] and 3.861 Å,[45] respectively. The lattice mismatch at the interface of LGO/KTO and NGO/KTO are 3.23% and 3.58% respectively, comparable to that of $PrAlO_3/SrTiO_3$ (3.41%) and $NdAlO_3/SrTiO_3$ (3.61%),[46] which have been experimentally prepared. In order to justify whether the 2DEG can be formed at the interface of LGO/KTO and NGO/KTO, the relative band alignment between the film oxides LGO and KTO, and between film oxides NGO and KTO are calculated by means of aligning their core energy levels of O 2s orbitals.[46] As can be seen from Fig. 2, the conduction band minimum (CBM) of LGO and NGO are both higher than that of the KTO substrate, suggesting that the 2DEG will most probably be formed and the electrons will be resident in the KTO side.

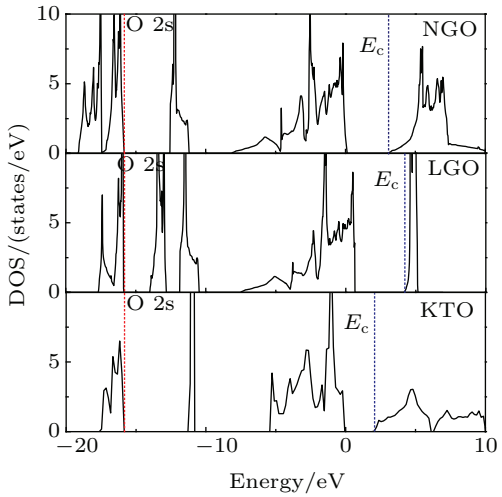


Fig. 2. Calculated density of states of bulk KTO, LGO, and NGO, where O 2s energy level is aligned to locate CBM.

3.2. Superlattice model

To investigate the intrinsic properties of the interface, the periodic superlattices are used due to no surface in this model. The band structure of $(LGO)_{5.5}/(KTO)_{5.5}$ and $(NGO)_{5.5}/(KTO)_{5.5}$ superlattice are obtained and shown in Fig. 3. From Figs. 3(a) and 3(b), it is noted that some conduction bands cross the Fermi level, indicating that both the superlattices are metallic. The band structure of NGO/KTO

around the Fermi level is quite similar to that of LGO/KTO; that is, the conduction bands' bottom states of the superlattices are mainly composed of Ta 5d orbitals. The light bands which are parabolic in the 2D k space are occupied by Ta d_{xy} singlet, and the only one heavy band is occupied by Ta $d_{xz/yz}$ doublet. To estimate the electron mobility, we calculate the electron effective mass (m^*) of the conduction band at the Γ point from the following equation:

$$m^* = \hbar^2 \left[\frac{\partial^2 \varepsilon(k)}{\partial k^2} \right]^{-1}. \quad (1)$$

The m^* is about $0.61m_e$ for the lower d_{xy} band parallel to the interface, while the m^* is substantially larger (about $11.72m_e$) for the upper $d_{xz/yz}$ band perpendicular to the interface. In contrast, for the LGO/STO and NGO/STO superlattice, the m^* is $0.87m_e$.[47,48] This implies that the electrons in KTO, with smaller effective mass, can move with higher mobility along the interface. These results are in good agreement with the previous studies,[36,39] indicating that the electron mobility can be improved by replacing STO substrate with KTO.

To investigate the spatial distribution of the electronic states in more detail, the orbital-resolved partial density of states (DOS) for Ta atoms of each layer in LGO/KTO superlattice is obtained and plotted in Fig. 4. The analysis of band structure shows that the Ta 5d orbitals split into nondegenerate d_{xy} state and two-fold degenerate $d_{xz/yz}$ state. The 2DEG originates from the d_{xy} electrons at the interface while the $d_{xz/yz}$ state makes little contribution to the metallic characteristics with an interfacial carrier density (n_s) of 1.25×10^{14} cm^{-2}. Compared with the small fraction of d_{xy} states, the occupancy of the $d_{xz/yz}$ band is dramatically enhanced in the interior of KTO. However, this band has quite a large electron effective mass, and plays little part in the two-dimensional electric conductivity. The spatial distribution of the 2DEG for NGO/KTO superlattice is almost the same as that for LGO/KTO.

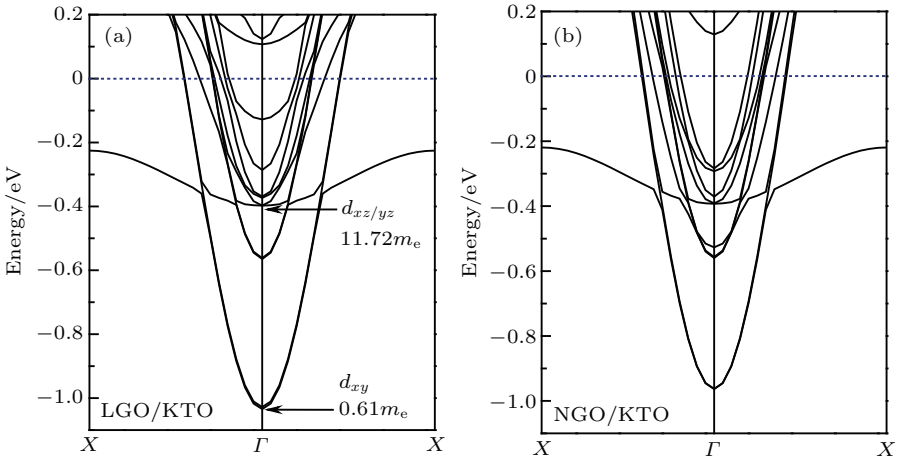


Fig. 3. Conduction bands near Fermi energy for (a) $(LGO)_{5.5}/(KTO)_{5.5}$ and (b) $(NGO)_{5.5}/(KTO)_{5.5}$ superlattice, with vertical dashed line indicating Fermi energy located at 0 eV.

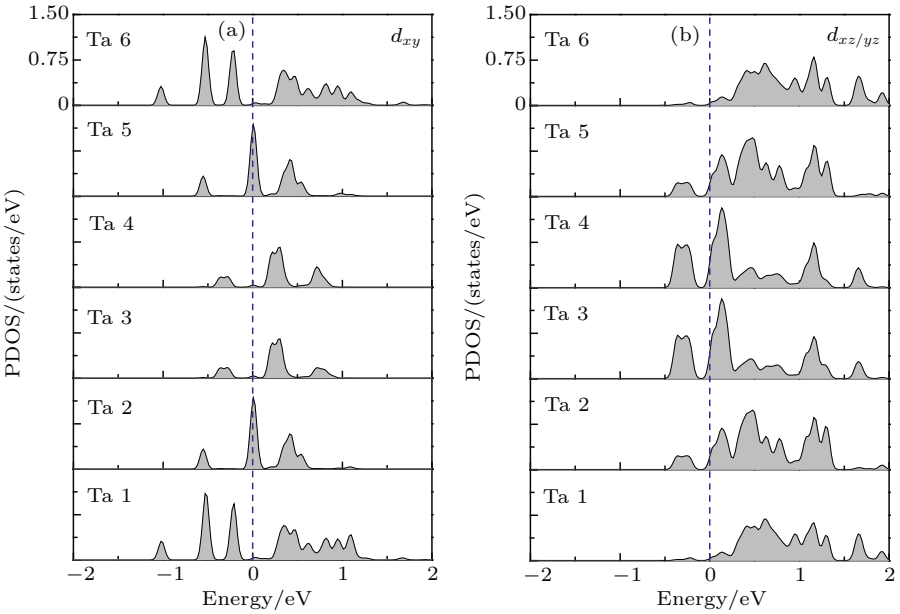


Fig. 4. Orbital-resolved partial DOS of (a) Ta d_{xy} states and (b) Ta $d_{xz/yz}$ states of each layer for $(LGO)_{5.5}/(KTO)_{5.5}$. Ta 1 is the Ta atom at the interface, Ta i is Ta atom of the i-th layer below it.

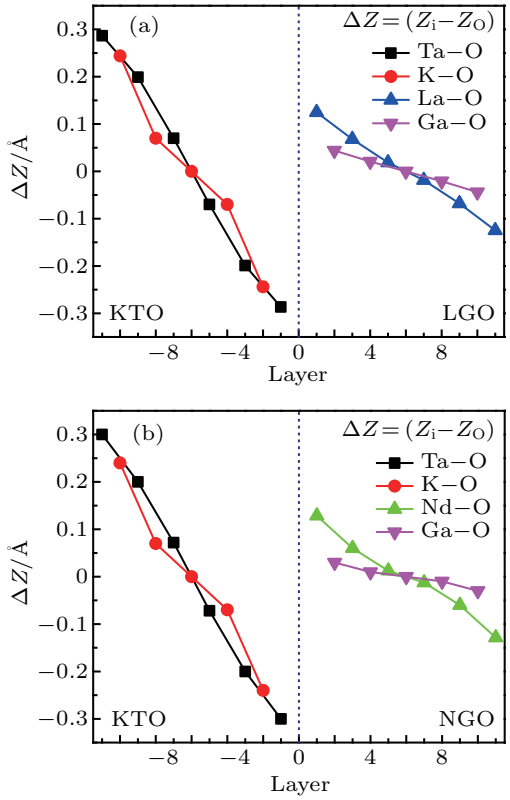


Fig. 5. Relative displacements of the cations and the oxygen anions in each layer for (a) $(LGO)_{5.5}/(KTO)_{5.5}$ and (b) $(NGO)_{5.5}/(KTO)_{5.5}$ superlattice along *c* axis.

The relative displacement between anion and cation in each layer along the *c* axis of the LGO/KTO and NGO/KTO superlattices are calculated, and shown in Fig. 5. It is obvious that there is a ferroelectric-like distortion of the oxygen octahedron on the KTO side; that is, oxygen ions move towards the interface while the cations move inward. And on the LGO (or NGO) side, the relative displacements are quite small due to no surface existing in the periodic superlattices. This behavior was also discovered in LAO/STO,[17] LGO/STO,[47] and NGO/STO[48] superlattices.

3.3. Thin film model

The advantage of the thin film model is that the calculated results compare well with the experimental observations by introducing the polar field in the thin film. Generally, a threshold thickness of the thin film is needed to form the metallic interface for the oxide heterostructures with STO substrate, such as LAO/STO, LGO/STO, and NGO/STO. In our calculations it is noted that the LGO/KTO (or NGO/KTO) systems are all metallic when the thickness of LGO (or NGO) varies from 1 u.c. to 10 u.c. Our calculations are in good agreement with previous results about LAO/KTO,[39] indicating that there exists no such threshold thickness in KTO-based heterostructure. It is worth mentioning that Wang *et al.* found that there is an overlap between the valence band maximum (VBM) and the CBM for the LAO/KTO system when the thickness of LAO is no less than 6 u.c.[39] However, such a behavior does not exist in our calculations, even when the thickness of LGO (or NGO) rises up to 10 u.c.

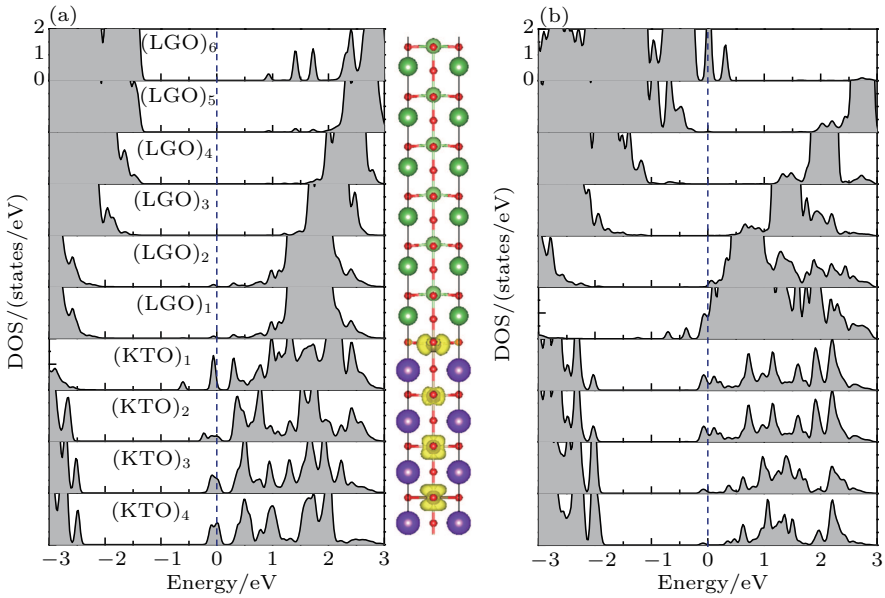


Fig. 6. Layer-projected partial DOS of (a) fully relaxed and (b) unrelaxed $(LGO)_6/(KTO)_{6.5}/(LGO)_6$ heterostructure, along with the conducting electron charge density from −1 eV to the Fermi level.

To understand the sources of this variation, the electronic structure of relaxed and unrelaxed $(AGO)_6/(KTO)_{6.5}/(AGO)_6$ heterostructure are obtained. The layer-projected partial DOS for the fully relaxed and unrelaxed $(LGO)_6/(KTO)_{6.5}/(LGO)_6$ system are compared as shown in Figs. 6(a) and 6(b). From Fig. 6(b), it is noted that the electrons contributed by LGO and KTO reside at the interface due to the polar discontinuity, resulting in the interfacial metallic states. In addition, the VBM of each layer of LGO shifts towards the Fermi level as the distance to the interface increases. The hole conducting states

are formed on the surface of GaO_2 layer because electrons are transferred from the surface to the interface. In contrast, even though there is also a shift of the VBM of each layer of LGO to higher energy for the optimized heterostructure, the VBM of O 2p state does not cross the Fermi energy and no charge transfer occurs. Accordingly, the LGO is insulating. These findings indicate that the LGO film of $(LGO)_6$/KTO heterostructure has a stronger polarization than the LAO film in $(LAO)_6$/KTO system mentioned before. This explains why there is no such overlapping between the VBM and the CBM in our calculation. As shown in Fig. 7, the strong polarization in the NGO film greatly neutralizes the build-in electric field in the $(NGO)_6$/KTO system, and the NGO becomes insulating, which is similar to the case of $(LGO)_6$/KTO. This phenomenon was also found for NGO/STO system in our previous calculation.[48] However, the biggest difference between NGO/STO and NGO/KTO heterointerface is that the former keeps insulating while the latter shows conducting states. This discrepancy can be explained by the fact that KTO plays a role of electron donor. The electrons of KTO occupy the conduction bands of Ta d_{xy} orbitals and form the 2DEG at the interface. As a result of the strong polarization, the interfacial carrier density of LGO/KTO and NGO/KTO in the thin film model are both about an order of magnitude lower than that in the superlattice model. An n_s of 10^{13} cm^{-2} matches well with that of LTO/KTO interface at 2 K, observed in experiment.[36] Here the calculated m^* is about $0.62m_e$ for the lowest Ta d_{xy} band.

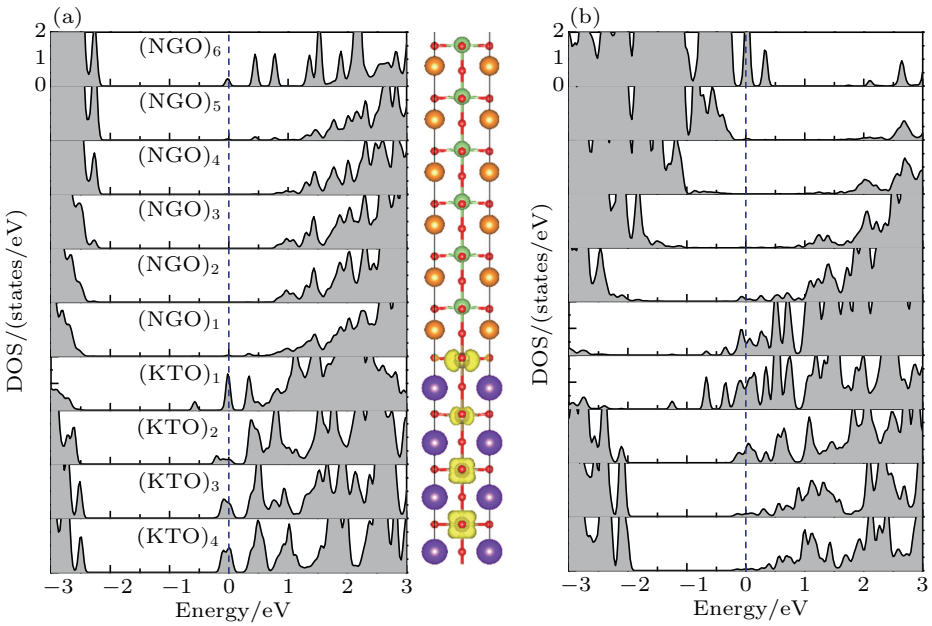


Fig. 7. Layer-projected partial DOS of (a) fully relaxed and (b) $(NGO)_6/(KTO)_{6.5}/(NGO)_6$ heterostructure, along with the conducting electron charge density from −1 eV to the Fermi level.

This analysis indicates that the lattice distortions have a great influence on electrical properties. Figure 8 displays the relative displacements between anions and cations in each layer along the c axis of the relaxed heterostructures. Due to the symmetry of the thin film model, only the relative displacements in a half of the supercell are plotted. It is found that large polar distortions do occur in both heterostructures. For the $(LGO)_6$/KTO system, the relative displacement in LaO layer increases from 0.25 Å to 0.33 Å with the increasing of the distance to the interface, while the relative displacement in GaO_2 layer decreases from 0.18 Å to 0.08 Å. Comparing with the $(LGO)_6$/STO system reported by Xu *et al.*,[49] the polar distortion in LGO of LGO/KTO is strong. This could be ascribed to the fact that the lattice mismatch of LGO/KTO is much larger than that of LGO/STO (only 1%). For the $(NGO)_6$/KTO system, the NdO layer is buckled to 0.27 Å–0.37 Å, and the GaO_2 layer is buckled to 0.18 Å–0.08 Å. The magnitude of the polar distortion is similar to that in $(LGO)_6$/KTO. In addition, for both of the KTO-based heterostructures the polarization in the KTO layer is stronger than that in STO layer of STO-based heterostructure.

To quantify the polarization strength, the polarization P within AGO film in AGO/KTO system is calculated from the following equation:[50,51]

$$P = \frac{e}{\Omega}\sum_{m=1}^{N} Z_m^* \delta z_m, \tag{2}$$

where N is the number of atoms in the unit cell, Ω is the volume of the AGO film, δz_m is the relative displacement between anion and cation in the m layer along the c axis. The calculated values of born effective charge Z_m^* are 4.42, 3.21, −2.49, and −2.57 for La, Ga, and O ions in the LaO and GaO_2 plane for the LGO in the tetragonal phase, respectively. For the NGO in the tetragonal phase, the Z_m^* are 4.48, 3.19, −2.49, and

−2.59 for Nd, Ga, and O ions in the NdO and GaO_2 planes, respectively. Figure 9 presents the polarization P of the AGO films for AGO/KTO heterostructures with different numbers of AGO unit cells. Figure 9 clearly shows a trend of polarization strength decreasing in the AGO film with the successive increase of the AGO film thickness. For comparison, we also calculate the polarization P within LGO film for LGO/STO system with 6 u.c. of LGO and 7 u.c. of LGO. This happens because the LGO/STO heterointerface becomes metallic beyond a critical thickness of 7 u.c. of LGO in our calculation. The resulting values are 45.26 μC/cm^2 and 41.57 μC/cm^2 for $(LGO)_6$/STO and $(LGO)_7$/STO, respectively. It is thus tempting to speculate that the critical LGO polarization is within 41.57 μC/cm^2–45.26 μC/cm^2. However, even when the thickness of LGO reaches 10 u.c. for LGO/KTO system, the calculated polarization is as high as 46.49 μC/cm^2. Clearly, the polarization of the LGO film is strong enough to totally counteract the build-in electric field. For the NGO/KTO system, the polarization of the NGO film is even stronger. The calculated P is 51.93 μC/cm^2 for the $(NGO)_{10}$/KTO heterostructure.

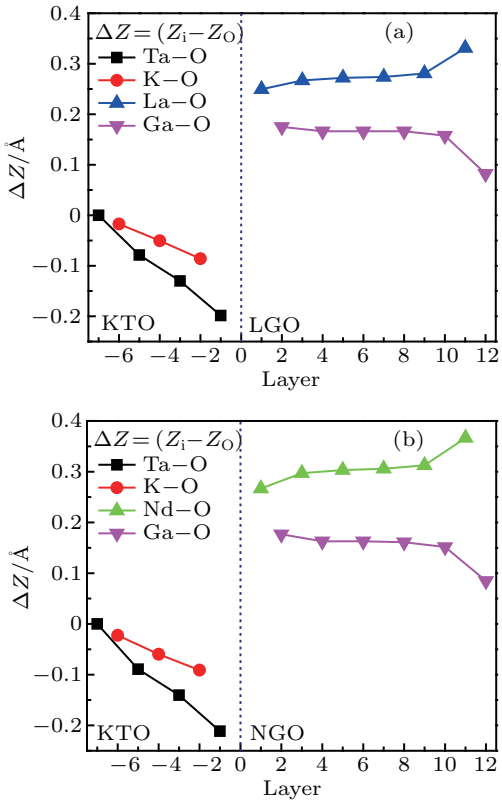


Fig. 8. Relative displacements of the cations and the oxygen anions in each layer for panel (a) $(LGO)_6/(KTO)_{6.5}/(LGO)_6$ and panel (b) $(NGO)_6/(KTO)_{6.5}/(NGO)_6$ heterostructure along the c axis.

Furthermore, the cleavage energy of LGO/KTO and NGO/KTO are calculated to evaluate the interfacial cohesion. The cleavage energy is given by[39]

$$E_{\rm cl} = \left(E_{\rm slab}^{\rm KTO} + E_{\rm slab}^{AGO} - E_{\rm HS}\right)/2A, \qquad (3)$$

where $E_{\rm slab}^{\rm KTO}$ and $E_{\rm slab}^{AGO}$ are the calculated total energy of KTO slab and LGO (or NGO) slab, respectively, which are built in the heterostructure by replacing the other part with vacuum. The $E_{\rm HS}$ represents the total energy of the heterostructure, and A represents the interface area. The calculated cleavage energy for LGO/KTO and NGO/KTO are 0.33 eV/Å^2 and 0.38 eV/Å^2 respectively. Both values are larger than 0.11 eV/Å^2 for LAO/KTO[39] and 0.19 eV/Å^2 for LAO/STO heterostructure.[52] This means that the interfacial cohesion of LGO/KTO and NGO/KTO is stronger. In other words, both of the heterointerfaces are theoretically stable and very likely to be formed in experiment.

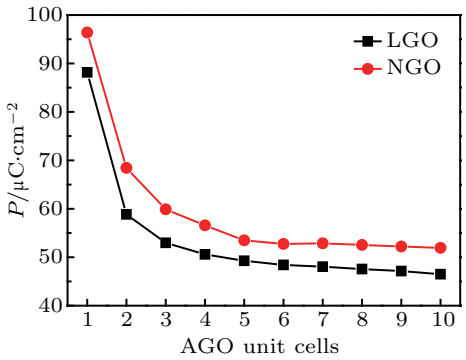


Fig. 9. Calculated polarization P in the AGO (A = La and Nd) films with respect to the AGO film thickness for the $(AGO)_m$/KTO/$(AGO)_m$ (m = 1–10) heterostructures.

4. Conclusions

In this work, the possibility of generating the 2DEG in two different models of LGO/KTO and NGO/KTO heterostructure is explored by using first-principles density functional calculations. The 2DEG with a high carrier density of 10^{14} cm^{-2} is produced at LGO/KTO and NGO/KTO heterointerface in the symmetric superlattice model. In the thin film model, all the heterointerfaces are found to be metallic without an insulator-to-metal transition. The interfacial carrier density of the 2DEG is about an order of magnitude lower than that in the superlattice model because large polar distortions in the LGO and NGO layers greatly screen the built-in electric field and prevent electrons from transferring to the interface. The partially filled Ta d_{xy} orbital is the origin of the 2DEG. The Ta d_{xy} electrons with smaller effective mass in KTO-based heterostructure are expected to move with higher mobility along the interface. Our calculations are helpful in understanding the 2DEG and have important implications for developing new heterostructure hosting superior 2DEG.

References

[1] Brinkman A, Huijben M, Van Zalk M, Huijben J, Zeitler U, Maan J C, Van der Wiel W G, Rijnders G, Blank D H A and Hilgenkamp H 2007 *Nat. Mater.* **6** 493
[2] Reyren N, Thiel S, Caviglia A D, Kourkoutis L F, Hammerl G, Richter C, Schneider C W, Kopp T, Ruetschi A S, Jaccard D, Gabay M, Muller D A, Triscone J M and Mannhart J 2007 *Science* **317** 1196
[3] Caviglia A D, Gariglio S, Reyren N, Jaccard D, Schneider T, Gabay M, Thiel S, Hammerl G, Mannhart J and Triscone J M 2008 *Nature* **456** 624

[4] Ohtomo A and Hwang H Y 2004 *Nature* **427** 423
[5] Cen C, Thiel S, Hammerl G, Schneider C W, Andersen K E, Hellberg C S, Mannhart J and Levy J 2008 *Nat. Mater.* **7** 298
[6] Thiel S, Hammerl G, Schmehl A, Schneider C W and Mannhart J 2006 *Science* **313** 1942
[7] Huijben M, Rijnders G, Blank D H A, Bals S, Van Aert S, Verbeeck J, Van Tendeloo G, Brinkman A and Hilgenkamp H 2006 *Nat. Mater.* **5** 556
[8] Nakagawa N, Hwang H Y and Muller D A 2006 *Nat. Mater.* **5** 204
[9] Herranz G, Basletic M, Bibes M, Carretero C, Tafra E, Jacquet E, Bouzehouane K, Deranlot C, Hamzic A, Broto J M, Barthelemy A and Fert A 2007 *Phys. Rev. Lett.* **98** 216803
[10] Kalabukhov A, Gunnarsson R, Borjesson J, Olsson E, Claeson T and Winkler D 2007 *Phys. Rev. B* **75** 121404
[11] Siemons W, Koster G, Yamamoto H, Harrison W A, Lucovsky G, Geballe T H, Blank D H A and Beasley M R 2007 *Phys. Rev. Lett.* **98** 196802
[12] Pavlenko N, Kopp T, Tsymbal E Y, Mannhart J and Sawatzky G A 2012 *Phys. Rev. B* **86** 064431
[13] Willmott P R, Pauli S A, Herger R, Schleputz C M, Martoccia D, Patterson B D, Delley B, Clarke R, Kumah D, Cionca C and Yacoby Y 2007 *Phys. Rev. Lett.* **99** 155502
[14] Salluzzo M, Gariglio S, Torrelles X, Ristic Z, Di Capua R, Drnec J, Sala M M, Ghiringhelli G, Felici R and Brookes N B 2013 *Adv. Mater.* **25** 2333
[15] Popovic Z S, Satpathy S and Martin R M 2008 *Phys. Rev. Lett.* **101** 256801
[16] Pentcheva R and Pickett W E 2008 *Phys. Rev. B* **78** 205106
[17] Li J C, Beltran J I and Munoz M C 1952 *Phys. Rev. B* **87** 5
[18] Du Y L, Wang C L, Li J C, Xu P P, Zhang X H, Liu J, Su W B and Mei L M 2014 *Chin. Phys. B* **23** 087302
[19] Basletic M, Maurice J L, Carretero C, Herranz G, Copie O, Bibes M, Jacquet E, Bouzehouane K, Fusil S and Barthelemy A 2008 *Nat. Mater.* **7** 621
[20] Cen C, Thiel S, Mannhart J and Levy J 2009 *Science* **323** 1026
[21] Singh-Bhalla G, Bell C, Ravichandran J, Siemons W, Hikita Y, Salahuddin S, Hebard A F, Hwang H Y and Ramesh R 2011 *Nat. Phys.* **7** 80
[22] Chen Y Z, Christensen D V, Trier F, Pryds N, Smith A and Linderoth S 2012 *Appl. Surf. Sci.* **258** 9242
[23] Plumb N C, Kobayashi M, Salluzzo M, Razzoli E, Matt C E, Strocov V N, Zhou K J, Shi M, Mesot J, Schmitt T, Patthey L and Radovic M 2017 *Appl. Surf. Sci.* **412** 271
[24] Chen Y Z, Pryds N, Sun J R, Shen B G and Linderoth S 2013 *Chin. Phys. B* **22** 116803
[25] Ishida H and Liebsch A 2008 *Phys. Rev. B* **77** 115350
[26] Kim J S, Seo S S A, Chisholm M F, Kremer R K, Habermeier H U, Keimer B and Lee H N 2010 *Phys. Rev. B* **82** 201407
[27] Perna P, Maccariello D, Radovic M, Scotti di Uccio U, Pallecchi I, Codda M, Marre D, Cantoni C, Gazquez J, Varela M, Pennycook S J and Miletto Granozio F 2010 *Appl. Phys. Lett.* **97** 152111
[28] Moetakef P, Cain T A, Ouellette D G, Zhang J Y, Klenov D O, Janotti A, Van de Walle C G, Rajan S, Allen S J and Stemmer S 2011 *Appl. Phys. Lett.* **99** 232116
[29] Annadi A, Putra A, Srivastava A, Wang X, Huang Z, Liu Z Q, Venkatesan T and Ariando 2012 *Appl. Phys. Lett.* **101** 231604
[30] Uccio U S d, Aruta C, Cantoni C, Gennaro E D, Gadaleta A, Lupini A R, Maccariello D, Marr D, Pallecchi I, Paparo D, Perna P, Riaz M and Granozio F M 2012 *Condens. Matter: Mater. Sci.* arXiv: 1206.5083 [cond-mat.mtrl-sci]
[31] Gunkel F, Skaja K, Shkabko A, Dittmann R, Hoffmann-Eifert S and Waser R 2013 *Appl. Phys. Lett.* **102** 071601
[32] Li C, Xu Q F, Wen Z, Zhang S T, Li A D and Wu D 2013 *Appl. Phys. Lett.* **103** 201602
[33] Kalabukhov A, Boikov Y A, Serenkov I T, Sakharov V I, Claeson T and Winkler D 2015 *J. Phys.: Condes. Matter* **27** 255004
[34] Wong F J, Baek S H , Chopdekar R V, Mehta V V, Jang H W, Eom C B and Suzuki Y 2010 *Phys. Rev. B* **81** 161101
[35] Wemple S H 1965 *Phys. Rev.* **137** A1575
[36] Zou K, Ismail-Beigi S, Kisslinger K, Shen X, Su D, Walker F J and Ahn C H 2015 *APL Mater.* **3** 036104
[37] Zhang H, Zhang H, Yan X, Zhang X, Zhang Q, Zhang J, Han F, Gu L, Liu B, Chen Y, Shen B and Sun J 2017 *ACS Appl. Mater. Interfaces* **9** 36456
[38] Zhang H, Yun Y, Zhang X, Zhang H, Ma Y, Yan X, Wang F, Li G, Li R, Khan T, Chen Y, Liu W, Hu F, Liu B, Shen B, Han W and Sun J 2018 *Phys. Rev. Lett.* **121** 116803
[39] Wang Y Q, Tang W, Cheng J L, Behtash M and Yang K S 2016 *ACS Appl. Mater. Interfaces* **8** 13659
[40] Koirala P, Gulec A and Marks L D 2017 *Surf. Sci.* **657** 15
[41] Kresse G and Furthmuller J 1996 *Phys. Rev. B* **54** 11169
[42] Perdew J P, Burke K and Ernzerhof M 1996 *Phys. Rev. Lett.* **77** 3865
[43] Monkhorst H J and Pack J D 1976 *Phys. Rev. B* **13** 5188
[44] Lee K S, Choi J H, Lee J Y and Baik S 2001 *J. Appl. Phys.* **90** 4095
[45] Annadi A, Putra A, Liu Z Q, Wang X, Gopinadhan K, Huang Z, Dhar S, Venkatesan T and Ariando 2012 *Phys. Rev. B* **86** 085450
[46] Yang K, Nazir S, Behtash M and Cheng J L 2016 *Sci. Rep.* **6** 9
[47] Wang F N, Li J C, Du Y L, Zhang X H, Liu H Z, Liu J, Wang C L and Mei L M 2015 *Appl. Surf. Sci.* **355** 1316
[48] Wang F N, Li J C, Zhang X M, Liu J, Zhao M L, Su W B, Wang C L and Mei L M 2018 *Comput. Mater. Sci.* **147** 87
[49] Xu Q F, Wu D and Li A D 2013 *Phys. Lett. A* **377** 577
[50] Zhong W, King-Smith R D and Vanderbilt D 1994 *Phys. Rev. Lett.* **72** 3618
[51] Behtash M, Nazir S, Wang Y Q and Yang K S 2016 *Phys. Chem. Chem. Phys.* **18** 6831
[52] Nazir S, Cheng J L, Behtash M, Luo J and Yang K S 2015 *ACS Appl. Mater. Interfaces* **7** 14294